

1 **Paleoclimate pattern effects constrain climate
2 sensitivity and future warming**

3 **V. T. Cooper^{1*}, K. C. Armour^{1,2}, G. J. Hakim¹, J. E. Tierney³, N. J. Burls⁴,**
4 **C. Proistosescu⁵, T. Andrews^{6,7}, W. Dong^{8,9}, M. T. Dvorak², R. Feng¹⁰, M. B.**
5 **Osman¹¹, Y. Dong¹²**

6 ¹Department of Atmospheric and Climate Science, University of Washington, Seattle, WA, USA

7 ²School of Oceanography, University of Washington, Seattle, WA, USA

8 ³Department of Geosciences, University of Arizona, Tucson, AZ, USA

9 ⁴Department of Atmospheric, Oceanic and Earth Sciences, George Mason University, Fairfax, VA, USA

10 ⁵Department of Climate, Meteorology, and Atmospheric Sciences, University of Illinois at

11 Urbana-Champaign, Champaign, IL, USA

12 ⁶Met Office Hadley Centre, Exeter, UK

13 ⁷School of Earth and Environment, University of Leeds, Leeds, UK

14 ⁸Cooperative Programs for the Advancement of Earth System Science, University Corporation for

15 Atmospheric Research, Boulder, CO, USA

16 ⁹NOAA/Geophysical Fluid Dynamics Laboratory, Princeton, NJ, USA

17 ¹⁰Department of Geosciences, University of Connecticut, Storrs, CT, USA

18 ¹¹Department of Geography, The University of Cambridge, Cambridge, UK

19 ¹²Department of Atmospheric and Oceanic Sciences, University of California Los Angeles, Los Angeles,

20 CA, USA

Corresponding author: *Vincent T. Cooper, vcooper@uw.edu

21 **Abstract**

22 Paleoclimates provide examples of past climate change that inform estimates of mod-
 23 ern warming from greenhouse-gas emissions, known as Earth's climate sensitivity. How-
 24 ever, differences between past and present climate change must be accounted for when
 25 inferring climate sensitivity from paleoclimate evidence [1–3]. The Pliocene (5.3–2.6 Ma),
 26 a warm epoch with atmospheric CO₂ concentrations similar to today, is a potential ana-
 27 log for modern warming [4]. Recent reconstructions indicate the Pliocene was 1°C warmer
 28 than previously thought [5, 6], implying higher climate sensitivity [5], supported by re-
 29 constructions of more global cooling from reduced CO₂ at the Last Glacial Maximum
 30 (LGM; 19–23 thousand years ago) [7–9]. However, these same reconstructions indicate
 31 large-scale patterns of paleoclimate temperature change differ strongly from modern pro-
 32 jections. Climate feedbacks and sensitivity depend on temperature patterns [e.g., 10–
 33 14], and such “pattern effects” must be accounted for when using paleoclimates to con-
 34 strain modern climate sensitivity [3]. Here we combine data-assimilation reconstructions
 35 with atmosphere models to show Earth's climate is more sensitive to Pliocene forcing
 36 than modern CO₂ forcing. Pliocene ice sheets, topography, and vegetation alter patterns
 37 of ocean warming and excite destabilizing cloud feedbacks, and LGM feedbacks are sim-
 38 ilarly amplified by the North American ice sheet. Accounting for paleoclimate pattern
 39 effects produces a best estimate (median) for modern climate sensitivity of 2.8°C, 66%
 40 range 2.4 – 3.4°C (90% CI: 2.1 – 4.0°C), substantially reducing uncertainty and nar-
 41 rowing projections of 21st-century warming.

42 **Main text**

43 The paleoclimate record constitutes a series of natural experiments with fundamen-
 44 tal insights into Earth's climate sensitivity. Using paleoclimate evidence to constrain the
 45 modern sensitivity to rising greenhouse-gas (GHG) concentrations requires accounting
 46 for differences in both climate forcings and feedbacks between the past and modern cli-
 47 mates [1–3]. A key driver of such feedback differences across past climates is variation
 48 in the spatial pattern of sea-surface temperature, i.e., “paleoclimate pattern effects” [3].
 49 Pattern effects are variations in climate sensitivity and feedbacks that depend on spa-
 50 tial patterns of temperature change [e.g., 10–14], and they arise in paleoclimate contexts
 51 when non-CO₂ forcings (such as ice sheets, topography, and vegetation) affect large-scale
 52 temperature patterns. Paleoclimate pattern effects can have major impacts on estimates
 53 of modern climate sensitivity if non-CO₂ forcings strongly influence the temperature pat-
 54 tern, thereby producing climate feedbacks that differ from those that govern modern warm-
 55 ing from GHG forcing [3].

56 The Pliocene (5.3–2.6 Ma) is the closest analog to near-term warming [4]. Its mid-
 57 Piacenzian warm period (c. 3.3–3.0 Ma), hereafter “Pliocene,” is the most recent epoch
 58 with atmospheric concentrations of CO₂ (near 400 ppm) that are similar to present day
 59 [15]. The magnitude of Pliocene warming thus provides an important constraint on the
 60 equilibrium climate sensitivity (ECS) of the modern climate, which is the steady-state
 61 response of global-mean near-surface air temperature to a doubling of atmospheric CO₂
 62 from preindustrial levels [2, 16]. Previous assessments of paleoclimate proxies report ap-
 63 proximately 3°C of global-mean Pliocene warming and an upper bound of 4°C relative
 64 to preindustrial conditions [2, 16]. However, recent reconstructions find a much warmer
 65 Pliocene, with central estimates of 4°C [5, 6]. This revision to Pliocene warming sug-

66 gests a much higher ECS of 4.8°C [5], implying increased likelihood of realizing the worst-
 67 case projections of 21st-century warming. But these globally resolved reconstructions tell
 68 us more than global means—they capture the spatial pattern of Pliocene warming, and
 69 this spatial information is essential to constraining modern ECS.

70 To infer modern ECS from Pliocene evidence, we must consider differences in both
 71 forcing and feedbacks between the Pliocene and present climate. The Pliocene has both
 72 elevated GHG levels [15, 17] as well as additional forcing from (i) reduced ice sheets over
 73 West Antarctica and Greenland, (ii) increased vegetation, especially over northern high
 74 latitudes, and (iii) changes in land-sea distribution [1, 2, 18, 19]. Previous work found
 75 that the Pliocene’s global-mean warming is mostly attributable to CO₂ [20–22]. How-
 76 ever, modeling studies show that the non-CO₂ forcings drive distinct climate responses
 77 especially at regional scales [20, 22–27], and that Pliocene temperature patterns may dif-
 78 fer substantially from those in response to modern CO₂ forcing [23], thereby producing
 79 different climate feedbacks. Accounting for such pattern effects in the Last Glacial Max-
 80 imum (LGM), a cold period 19–23 ka, led to stronger constraints on modern ECS [3].
 81 The key question addressed here is: would accounting for Pliocene pattern effects also
 82 strengthen constraints on modern ECS?

83 We quantify Pliocene pattern effects by synthesizing proxy data with climate mod-
 84 els, and we use these results to revise estimates of modern ECS and 21st-century warm-
 85 ing. Spatially complete reconstructions of the Pliocene [5, 6] from paleoclimate data as-
 86 similation [7, 8, 28] are used in numerical simulations with five atmospheric general cir-
 87 culation models (AGCMs) to quantify relationships between temperature patterns and
 88 climate feedbacks [e.g., 3, 11]. We analyze differences between feedbacks in the Pliocene
 89 compared to modern warming from CO₂. We then combine our Pliocene results with
 90 an investigation of the LGM [3], and we quantify the impacts of the feedback differences
 91 on estimates of modern ECS and projections of 21st-century warming.

92 Paleoclimate pattern effects and modern ECS

93 Modern ECS, climate feedbacks, and paleoclimate pattern effects are related through
 94 the global-mean energy balance,

$$95 \Delta N = \Delta F + \lambda \Delta T, \quad (1)$$

96 where ΔN is the change in top-of-atmosphere radiative balance; ΔF is the “effective”
 97 radiative forcing, i.e., the change in net downward radiative flux after atmospheric ad-
 98 justments to imposed perturbations, excluding radiative responses to changing surface
 99 temperature [16]; λ is the net climate feedback (negative for stable climates); and ΔT
 100 is the change in near-surface air temperature. All values are global means, and differ-
 101 ences (Δ) are relative to the preindustrial baseline. When the forcing is a doubling of
 102 preindustrial CO₂ concentrations (2xCO₂), and the climate reaches equilibrium ($\Delta N =$
 103 0), the resulting ΔT is the modern ECS:

$$104 \text{ECS} = -\Delta F_{2x\text{CO}_2} / \lambda_{2x\text{CO}_2}, \quad (2)$$

105 where $\Delta F_{2x\text{CO}_2}$ is the effective radiative forcing and $\lambda_{2x\text{CO}_2}$ is the net feedback from mod-
 106 ern CO₂ doubling. Increasingly negative values of λ indicate more-stable climates and
 107 lower ECS.

Paleoclimate pattern effects ($\Delta\lambda$) are quantified as the difference between λ_{2xCO_2} and a paleoclimate feedback, e.g., the Pliocene feedback (λ_{Plio}), due to differences in the spatial patterns of warming:

$$\Delta\lambda = \lambda_{2xCO_2} - \lambda_{Plio}. \quad (3)$$

$\Delta\lambda$ also can vary with global-mean temperature [e.g., 2, 3, 29]. However, this temperature dependence can be omitted for the Pliocene due to similar levels of global warming from Pliocene and $2xCO_2$ forcings [2] and is relatively small for LGM levels of global cooling [3, 30].

Modern ECS and λ_{2xCO_2} can be constrained by estimating λ_{Plio} and $\Delta\lambda$, then combining Equations 2 and 3:

$$ECS = -\Delta F_{2xCO_2}/(\lambda_{Plio} + \Delta\lambda). \quad (4)$$

$\Delta\lambda$ depends on spatial patterns of Pliocene temperature anomalies, for which we use state-of-the-art reconstructions from data assimilation [5, 6] as boundary conditions for simulations using five AGCMs, as described in the following section.

122 Pliocene pattern effects constrained by data assimilation

123 Patterns of Pliocene sea-surface temperature

In Fig. 1, we compare the projected sea-surface temperature (SST) anomalies from modern $2xCO_2$, based on the multi-model mean of quasi-equilibrium simulations in LongRunMIP [31], with the various Pliocene reconstructions from “plioDA” [5] and ref. [6] that we use to quantify Pliocene pattern effects. The Pliocene patterns include the best estimates from plioDA [5] and ref. [6], as well as alternate plioDA reconstructions that test structural uncertainty and endmembers of the plioDA ensemble (Fig. 1; Fig. S1–S4) (Methods). The reconstructions use paleoclimate data assimilation [7, 8, 28], which optimally combines dynamical constraints from model “priors” with proxy data. Data assimilation results depend on specific aspects of the methods, model priors [32], and observations.

To address reconstruction uncertainty, we analyze pattern effects across a wide range of possible Pliocene temperature patterns that use different assimilation methods, model priors, and subsets of proxy data. Focusing on sensitivity to the model prior, the “PlioMIP2 Prior” version of plioDA uses 14 PlioMIP2 simulations [33] to inform its prior. The “Perturbed Cloud Prior” uses 21 simulations that are designed to capture Pliocene temperature gradients by substantially altering models’ cloud physics [34–36]. Focusing on sensitivity to the proxy network, the “PlioVar Data” version restricts data to the KM5c interglacial [37], and we also test endmembers of the plioDA ensemble (Fig. S4) (Methods). Ref. [6] and plioDA [5] have partially overlapping proxy networks, model priors (both best estimates include simulations from PlioMIP2), and assimilation methods (ensemble Kalman filter); however, there are substantial differences between the two reconstruction efforts in terms of the proxies included, model priors, and methods (e.g., forward modeling of proxies in plioDA) that lead to differences in their results [5] (Fig. 1b,f).

Despite the substantial uncertainty in the details of the Pliocene SST patterns shown in Fig. 1, the reconstructions all have two common features that distinguish the Pliocene from the modern response to $2xCO_2$: the Pliocene has amplified SST warming in the South-

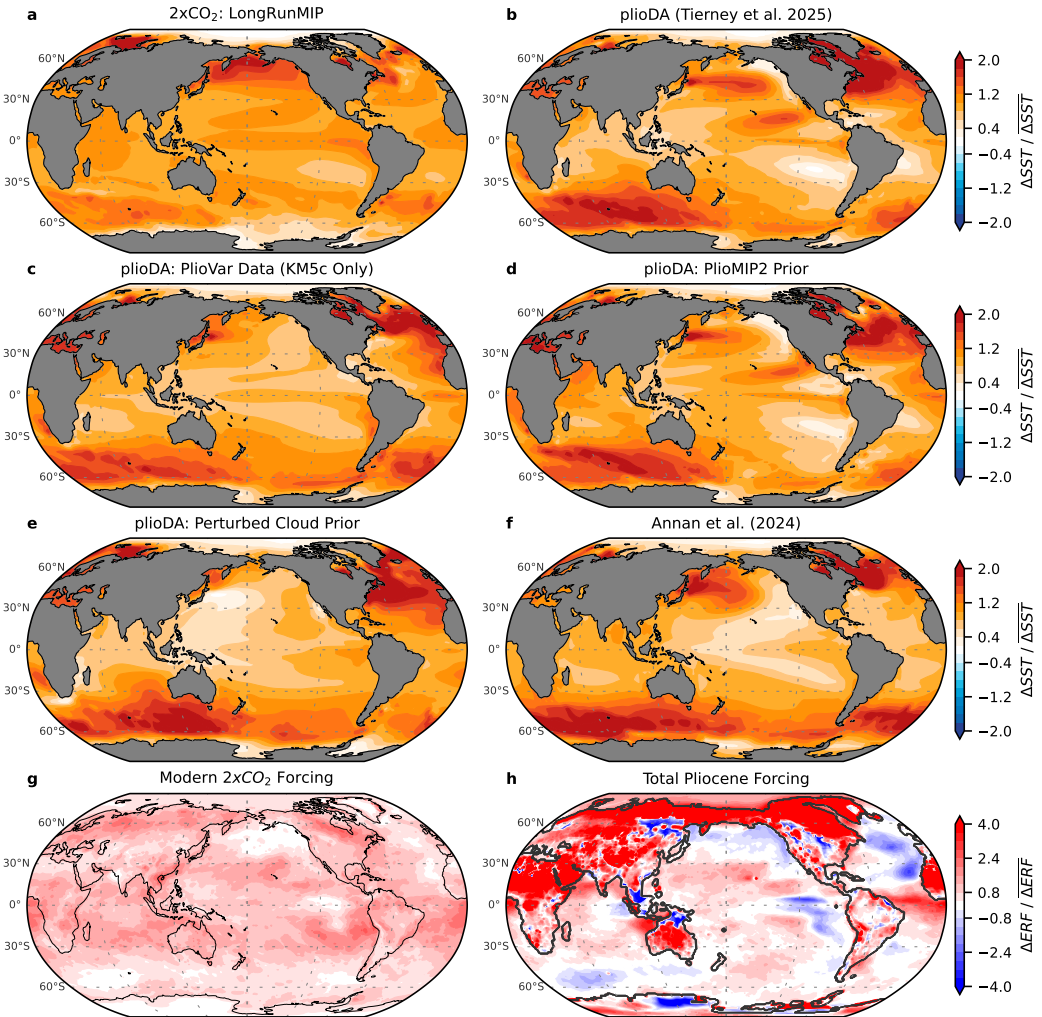


Figure 1. Patterns of sea-surface temperature (SST) anomalies and effective radiative forcing (ERF). (A) Multi-model mean of modern SST response to $2\times\text{CO}_2$ in quasi-equilibrium simulations from LongRunMIP [31]. (B–F) Data-assimilation reconstructions from: (B) plioDA best estimate [5]; alternate plioDA using (C) only the PlioVar proxy data representing the KM5c interglacial, (D) only the PlioMIP2 prior, or (E) only the perturbed-cloud prior; and (F) best estimate from ref. [6]. ERF from (G) modern $2\times\text{CO}_2$ and (H) Pliocene total forcing, including greenhouse gases, reduced Greenland and Antarctic ice sheets, sea level, and vegetation [23]. All panels show annual-mean anomalies, and local values are divided by global means. Pliocene SSTs are infilled to modern coastlines.

ern Ocean and the North Atlantic Ocean (Fig. 1; Fig. S1). The distinct Pliocene warming pattern is driven by the distinct spatial pattern of Pliocene *forcing* (Fig. 1h) [23], which arises from the Pliocene's non-CO₂ forcings (changes in ice sheets, topography, and vegetation) and differs substantially from the relatively uniform forcing produced by CO₂ alone (Fig. 1g). The connection between the non-CO₂ Pliocene forcings and the SST patterns they produce has been demonstrated in coupled climate models [23], which we return to in the Discussion.

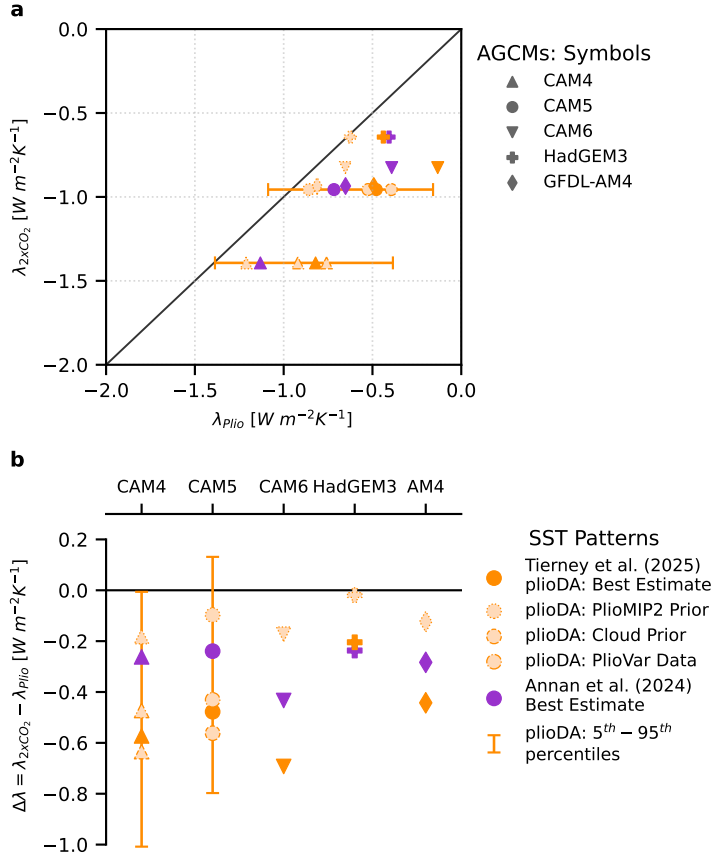


Figure 2. Net climate feedbacks (λ) and Pliocene pattern effect ($\Delta\lambda$). Note that each legend applies to both panels; different atmospheric general circulation models (AGCMs) are denoted by symbols, and different Pliocene warming patterns are denoted by colors and borders. (a) Scatter plot of λ_{2xCO_2} versus λ_{Plio} for each AGCM and Pliocene pattern, with $\lambda_{2xCO_2} = \lambda_{Plio}$ shown as solid line. (b) Pliocene pattern effect, $\Delta\lambda = \lambda_{2xCO_2} - \lambda_{Plio}$, using values in panel a. Error bars for plioDA represent endmembers of the ensemble reconstruction (Methods).

157 Quantifying feedbacks and pattern effects

We estimate the net climate feedback, λ , for each warming pattern in Fig. 1 using AGCM simulations with prescribed SST and sea-ice concentration (SIC) (Methods). Following ref. [3], we begin with a control simulation using the preindustrial “baseline” pattern [8]. We repeat the AGCM simulations, changing only the SST and SIC to the 2xCO₂ pattern from LongRunMIP (Fig. 1a) and to each of the Pliocene patterns (Fig. 1b–e; SIC in Fig. S2–S4). We hold the forcings constant at modern levels across all sim-

164 ulations to isolate the radiative response to changes in surface temperature (Methods).
 165 For each simulation, we calculate ΔN and ΔT relative to the preindustrial baseline, and
 166 the net feedback is $\lambda = \Delta N / \Delta T$ from Eq. 1 with $\Delta F = 0$.

167 In Fig. 2, we compare λ_{2xCO_2} with λ_{Plio} and quantify Pliocene pattern effects ($\Delta\lambda$).
 168 In all five AGCMs, λ_{Plio} is more positive (destabilizing) than λ_{2xCO_2} , which means that
 169 the climate system is more sensitive to Pliocene forcing than it is to modern $2xCO_2$ forcing.
 170 We test whether this result is robust despite uncertainties in atmospheric model physics
 171 and Pliocene reconstructions by running the simulations in CAM4, CAM5, CAM6, GFDL-
 172 AM4, and HadGEM3-GC3.1-LL, and by testing three different Pliocene patterns (Fig
 173 1B,D,F) in all five AGCMs. We test additional Pliocene patterns, including the 5th and
 174 95th percentiles of the plioDA ensemble (Fig. S4), in CAM4 and CAM5 (Methods). De-
 175 spite the uncertainties in Pliocene SST patterns and atmospheric model physics, there
 176 is a clear Pliocene pattern effect with $\Delta\lambda < 0$ (Fig. 2b), albeit with uncertain magni-
 177 tude.

178 In summary, the Pliocene warming pattern excites more positive (destabilizing) cli-
 179 mate feedbacks compared to the $2xCO_2$ warming pattern ($\lambda_{Plio} > \lambda_{2xCO_2}$), i.e., the Pliocene
 180 pattern effect is negative ($\Delta\lambda < 0$). As will be shown below, the negative pattern ef-
 181 fect indicates that positive feedbacks amplifying Pliocene warming do not play an equiv-
 182 alent role in the modern climate's response to greenhouse-gas forcing. Accounting for
 183 this negative Pliocene pattern effect would lead to lower estimates of modern ECS and
 184 future warming (Eq. 4) [3].

185 Discussion

186 Mechanisms responsible for Pliocene pattern effects

187 To diagnose the mechanisms contributing to more-positive climate feedbacks in the
 188 Pliocene, we first use radiative kernels to assess each component feedback within the AGCM
 189 simulations (Methods) [38]. We find that the cloud feedback (λ_{cloud}), namely the short-
 190 wave component associated with low clouds, is the dominant driver of $\lambda_{Plio} > \lambda_{2xCO_2}$
 191 (Fig. S5–S6). The combined lapse-rate and water-vapor feedbacks make an additional
 192 contribution to more-positive λ_{Plio} (Fig. S5). Next, we inspect the spatial distribution
 193 of the Pliocene's more-positive cloud feedbacks to understand their source.

194 In Fig. 3, we compare the spatial patterns of λ_{cloud} in the Pliocene versus $2xCO_2$.
 195 The most pronounced differences are over the Southern Ocean (Indian sector) and the
 196 North Atlantic. The zonal mean of $\Delta\lambda_{cloud}$ (Fig. 3a) illustrates that the Pliocene's ex-
 197 tratropical cloud feedbacks are responsible for $\lambda_{Plio} > \lambda_{2xCO_2}$, supported by extratrop-
 198 ical lapse-rate feedbacks (Fig. S9). Comparing Fig. 3's λ_{cloud} with Fig. 1's SST patterns
 199 (zonal mean SST in Fig. S10), we see that the regions with amplified Pliocene SST anom-
 200 alies are approximately collocated with the amplified Pliocene λ_{cloud} . That is, amplified
 201 SST anomalies in the extratropics are responsible for more-positive feedbacks in the Pliocene,
 202 which is consistent with a similar analysis of the Last Glacial Maximum [3]. When SST
 203 warming is strongly amplified in the extratropics compared to the SST warming in trop-
 204 ical regions of atmospheric deep convection (e.g., the west Pacific warm pool), tropospheric
 205 stability is decreased and low-cloud cover is reduced, which is a positive feedback on the
 206 initial warming [3, 13, 39]. Past studies of the Pliocene emphasize the zonal SST in the

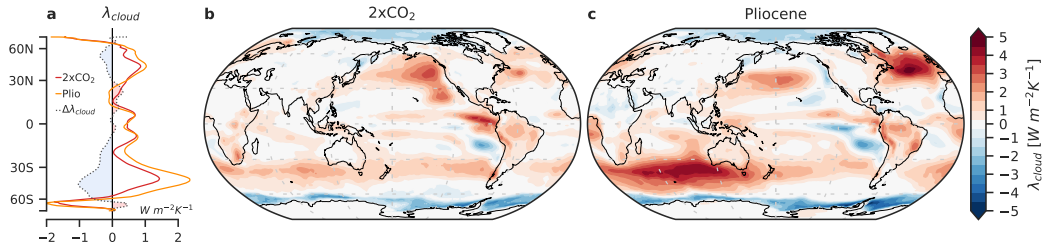


Figure 3. Cloud feedbacks from modern CO₂ forcing versus Pliocene warming.

(a) Zonal means of panels b, c, and their difference, $\Delta\lambda_{\text{cloud}}$; negative values of $\Delta\lambda_{\text{cloud}}$ contribute to the negative Pliocene pattern effect. (b–c) Spatial distributions of cloud feedbacks, $\lambda_{\text{cloud}} = \Delta N_{\text{local}}/\overline{\Delta T}$, where ΔN_{local} is the local anomaly in top-of-atmosphere radiation attributable to cloud feedbacks (estimated with radiative kernels), and $\overline{\Delta T}$ is the global-mean T anomaly. Multi-model mean of (b) λ_{cloud} using the LongRunMIP 2xCO₂ pattern and (c) multi-pattern mean λ_{cloud} from Pliocene patterns in Fig. 1b,d,f (plioDA best estimate [5], alternate plioDA using only the PlioMIP2 prior, and ref. [6] best estimate; these patterns were tested in all atmosphere models). All panels show multi-model means across atmosphere models.

tropical Pacific and meridional temperature gradients [5, 21, 40–44], while we find that the amplification of warming in the North Atlantic and especially the Southern Ocean are the dominant features that distinguish Pliocene feedbacks from the modern response to 2xCO₂.

The final and essential aspect of the mechanism is that amplified warming in the Southern Ocean and North Atlantic is due to non-CO₂ forcings (ice sheets, vegetation, and topography), as shown in Fig. S11. This attribution has been illustrated by simulations in coupled climate models that separate the SST response to Pliocene CO₂ versus non-CO₂ forcings [e.g., 20, 22, 23, 33]. Pliocene warming in the North Atlantic is amplified by the closure of ocean gateways (Bering Strait and Canadian Archipelago) through changes in the Atlantic Meridional Overturning Circulation (AMOC) [24], and it is further amplified by reductions in ice sheets [26]. Amplified warming in the Southern Ocean is associated with the reduced Antarctic Ice Sheet and topography through changes in ocean circulation [23, 45]. While amplified warming of the Southern Ocean appears in all reconstructions (Fig. 1), its magnitude is uncertain due to sparse proxy data, and this uncertainty makes a large contribution to our spread in $\Delta\lambda$ (Fig. S8–S10). Compared to coupled models, both the North Atlantic and Southern Ocean SST features are even more pronounced in data-assimilation reconstructions constrained by paleoclimate proxies (Fig. 1) [5, 6]. Thus coupled models are essential for illustrating mechanisms of paleoclimate pattern effects, and incorporating observational constraints through data assimilation is key to producing reliable SST patterns and constraining $\Delta\lambda$.

While our comparison of the Pliocene versus modern 2xCO₂ uses the LongRunMIP pattern [31], we note that there is substantial uncertainty in the projected SST pattern from 2xCO₂. However, because Pliocene and LGM pattern effects arise from how non-CO₂ forcings shape paleoclimate temperature patterns, we expect conclusions about $\Delta\lambda$ to be relatively insensitive to uncertainty in the SST pattern from CO₂ forcing. Furthermore, ref. [46] finds that the feedback uncertainty from CO₂-forced SST patterns

is only 10% of the total feedback spread across different models. That result emphasizes the importance of using multiple atmospheric models to quantify $\Delta\lambda$ and that the feedback spread from 2xCO₂ patterns is small compared to that arising from the Pliocene reconstructions. We test whether results are sensitive to the 2xCO₂ pattern and find this uncertainty does not affect the conclusions (Methods).

In summary, non-CO₂ forcings from ice sheets, topography, and vegetation altered the spatial pattern of ocean warming, in turn producing positive cloud feedbacks in the extratropics that strongly amplified global warming during the Pliocene (Fig. 3). Because of these amplifying feedbacks, more of the Pliocene warming was caused by non-CO₂ forcings than previously thought, meaning that less of the warming is attributable to elevated CO₂ alone. Since these amplifying feedbacks from non-CO₂ forcing do not play a role in the modern response to 2xCO₂ alone, we now show that accounting for the Pliocene pattern effect lowers estimates of modern ECS and reduces the likelihood of worst-case projections for 21st-century warming.

Modern climate sensitivity and 21st-century warming

To constrain modern ECS with paleoclimate evidence, we first infer climate feedbacks during a paleoclimate period from changes in Earth's energy budget, and then we account for differences relative to the modern response to 2xCO₂ [1–3]. Measures of climate sensitivity depend on the timescale of interest, and we follow ref. [2], hereafter "SW20," in focusing on the 150-year timescale of "effective" climate sensitivity (S), and in treating slow paleoclimate feedbacks, e.g., ice sheets, as radiative forcings [1].

First, we estimate λ_{Plio} by applying Equation 1 to the Pliocene (Methods). We update ΔT_{Plio} from SW20's values of 3.0 ± 1.0 °C (1σ) to plioDA's result of $\Delta T_{\text{Plio}} = 4.1 \pm 0.6$ °C (1σ). We also update the non-GHG (greenhouse gas) effective radiative forcing to $\Delta F_{\text{NonGHG}} = 1.7 \pm 1.0$ (1σ) W m⁻² [23]. Given that $\Delta F_{\text{GHG}} \approx 2.2$ W m⁻² [2, 23], we have a central estimate of total $\Delta F_{\text{Plio}} = 3.9$ W m⁻² and $\lambda_{\text{Plio}} \approx -1.0$ W m⁻² K⁻¹ (Methods).

The novel aspect of the modern ECS constraint in this study is the inclusion of paleoclimate pattern effects for the Pliocene ($\Delta\lambda$; Eq. 3 and 4) and the synthesis with pattern effects for the Last Glacial Maximum [3]. We combine uncertainty across SST patterns and atmospheric models (Fig. 2; Methods), which produces a central estimate for Pliocene pattern effects of $\Delta\lambda = -0.37 \pm 0.32$ (1σ) W m⁻² K⁻¹. We adapt the Bayesian framework of SW20 to include Pliocene $\Delta\lambda$, following ref. [3] (Methods).

In Fig. 4a, we show the S likelihoods from Pliocene evidence alone. For comparison, we include the original SW20 results and the likelihood with updated Pliocene global-mean ΔT and ΔF_{NonGHG} but excluding Pliocene pattern effects. As seen in Fig. 4a, the updates from the *global-mean* information alone (excluding $\Delta\lambda$) suggest a much higher ECS [5]. However, the *spatial information* in the Pliocene reconstructions—quantified as $\Delta\lambda$ —has a larger and opposite impact. Including $\Delta\lambda$ shifts the maximum likelihood from 3.7°C to 2.7°C and substantially reduces the high tail of the distribution.

We now revise the best estimate for modern ECS by combining the Pliocene with the additional lines of evidence in SW20: the Last Glacial Maximum (LGM), the historical record (c. 1870–present), and process understanding (Methods) (Fig. 4b). We

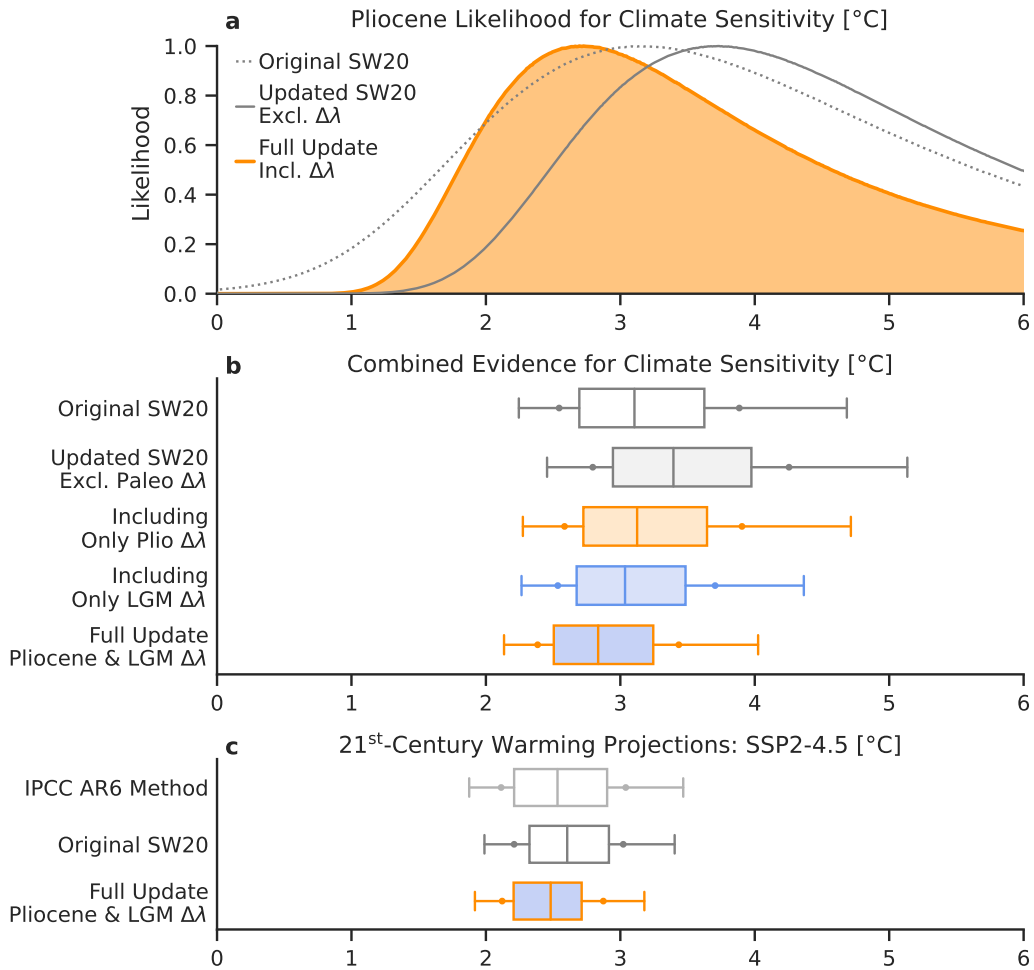


Figure 4. Modern climate sensitivity and 21st-century warming, accounting for paleoclimate pattern effects ($\Delta\lambda$). (a) Pliocene-only likelihoods (dotted) from SW20 [2]; (gray) including updates to ΔT_{Plio} and ΔF_{Plio} but excluding pattern effects ($\Delta\lambda$); (orange) fully updated SW20 including $\Delta\lambda$. **(b)** Posterior probability density functions (PDFs) after combining lines of evidence: (gray, white fill) SW20, (gray) SW20 with updated paleoclimate ΔT and ΔF but excluding $\Delta\lambda$, (orange) including $\Delta\lambda$ only for the Pliocene, (blue) $\Delta\lambda$ only for the Last Glacial Maximum (LGM) [3], and (orange, blue fill) Full Update including Pliocene and LGM $\Delta\lambda$. Panels **a–b** show effective climate sensitivity (S), as in SW20. **(c)** Projected global warming from the FaIR model [47], measured as mean anomaly over 2081–2100 relative to 1850–1900 mean, using climate sensitivity distributions from IPCC AR6 [16], SW20, and the Full Update in panel **b**. Line caps indicate 5th to 95th percentiles, dots indicate 66% *likely* range, box indicates 25th to 75th percentiles, and line indicates median.

first show SW20's results, then we include paleoclimate updates only to global-mean quantities (i.e., excluding $\Delta\lambda$), which increases ECS substantially. We then include $\Delta\lambda$ from only the Pliocene or LGM [3], and finally we combine our results for Pliocene and LGM $\Delta\lambda$ to provide a best estimate that fully accounts for paleoclimate pattern effects and their uncertainties. Once again, *global-mean* paleoclimate updates increase ECS, while the *spatial information* from pattern effects is more impactful and leads to much stronger overall constraints, particularly for the upper bound. The revised best estimate (median) for modern ECS becomes 2.8°C , with a 66% range of $2.4\text{--}3.4^{\circ}\text{C}$ (90% CI: $2.1\text{--}4.0^{\circ}\text{C}$) (Fig. 4b; Table S3). This range represents a major update to the upper bounds in SW20 [2] and the IPCC Sixth Assessment report (AR6) [16], while our lower bound confirms those assessments. For comparison with SW20's robustness tests, we find a 66% robust range of $2.6\text{--}3.8^{\circ}\text{C}$ (90% CI: $2.3\text{--}4.6^{\circ}\text{C}$), which also represents a much stronger constraint compared to the 95th percentile of 5.7°C in SW20's robust range.

Importantly, our updates to modern ECS also reduce uncertainty in projections of 21st-century warming. Fig. 4c shows the 2081–2100 mean warming relative to 1850–1900 projected by the FaIR model [47], a climate emulator that produced projections for IPCC AR6, under the SSP2-4.5 emissions scenario [16]. FaIR's large ensemble is calibrated to match the historical record through 2022 while sampling the full range of uncertainty in ECS [47]. We first revise the FaIR ensemble's ECS distribution to match SW20, which produces a minor change (Methods). We then use our fully updated ECS distribution with the FaIR model (Fig. 4b), which yields a median of 2.5°C for end-of-century warming (relative to preindustrial) and substantially reduces uncertainty in the upper bound of warming projections, with a 66% *likely* range of $2.1\text{--}2.9^{\circ}\text{C}$ (90% CI: $1.9\text{--}3.2^{\circ}\text{C}$).

Pliocene pattern effects arise from changes in ice sheets, vegetation, and topography that amplify SST warming in the extratropics, in turn leading to cloud feedbacks that further amplify global warming. Recent work on the Last Glacial Maximum also found that ice sheets amplify extratropical SST cooling, similarly leading to positive cloud feedbacks [3]. The modern climate feedback from CO₂ alone (in the absence of ice sheet, vegetation, and topography changes) is more stabilizing than the feedbacks associated with the Pliocene and LGM.

Updating *global mean* Pliocene and LGM temperatures based on the latest state-of-the-art reconstructions, while neglecting pattern effects, appears to suggest substantially higher estimates of *climate sensitivity* compared to SW20 [2] and IPCC AR6 [16]. However, our results show that including *spatial information* from those same reconstructions leads to the opposite conclusion, such that paleoclimates now provide much stronger constraints on the modern climate's sensitivity to CO₂ and projected warming. We note that our 21st-century projections assume ice sheets will not be lost this century. An important corollary to our results is that a major shift in the modern warming pattern, e.g., caused by loss of the West Antarctic Ice Sheet [23, 27, 45], could activate positive feedbacks on longer timescales in the modern climate similar to those that amplified global warming during the Pliocene.

319 **Methods**320 **AGCM simulations**

321 Following ref. [3], estimating paleoclimate $\Delta\lambda$ (Eq. 3) in AGCMs requires three
 322 simulations that differ only in their SST/SIC boundary conditions while all other forcings
 323 are constant at modern levels, similar to “amip-piForcing” simulations [12, 48].

324 The three categories of AGCM simulations are: **(a)** Preindustrial baseline, for which
 325 we use the Late Holocene (0–4 ka) [8]; **(b)** 2xCO₂, for which we use the multi-model
 326 mean of quasi-equilibrium 2xCO₂ simulations in LongRunMIP [31]; **(c)** Pliocene, for which
 327 we use the various reconstructions described in the main text (Fig. 1; Fig. S1–S3). In
 328 CAM4 and CAM5, we also test the 5th and 95th percentiles of the plioDA ensemble (Fig.
 329 S4); ensemble members are ranked by estimating λ_{Plio} with CAM4 Green’s functions [39].
 330 SST/SIC boundary conditions are prepared as described in ref. [3]. We use plioDA’s SIC
 331 for ref. [6], as no SIC is provided by the latter; this approach is supported by similar ΔT_{Plio}
 332 in both reconstructions.

333 For each AGCM, we compute anomalies in simulations **(b)** and **(c)** relative to **(a)**.
 334 Simulations are 30 years, and we analyze means over the final 25 years for CAM4 (2°
 335 resolution), CAM5.3 (2°), CAM6.0 (2°) [49], and HadGEM3-GC3.1-LL (N96, 135 km)
 336 [50], or the final 30 of 31 years for GFDL-AM4.0 (C96, 100 km) [51]. Results are included
 337 in Tables S1–S2. As described in ref. [3], we test sensitivity of $\Delta\lambda$ to the 2xCO₂ pat-
 338 tern by computing an alternate $\Delta\lambda_{150\text{yr}}^{\text{Alt}}$, which uses the 150-year regression of abrupt
 339 CO₂-forcing simulations in the parent coupled models corresponding to each AGCM in-
 340 stead of our $\lambda_{2\text{xCO}_2}$. Each coupled model produces a distinct warming pattern over the
 341 150-year period, thus $\Delta\lambda_{150\text{yr}}^{\text{Alt}}$ samples uncertainty in CO₂-warming patterns. This test
 342 confirms our finding of $\Delta\lambda < 0$ (Table S1–S2) and produces ECS constraints that agree
 343 with our main result within 0.1°C (Table S3). We decompose λ into component feed-
 344 backs (Planck, lapse rate, water vapor, surface albedo, shortwave cloud, and longwave
 345 cloud) using CAM5 radiative kernels [52], following ref. [38] (Fig. S5–S8).

346 **Constraining modern climate sensitivity**

347 Modern climate sensitivity is the steady-state response of global-mean T to dou-
 348 bling preindustrial CO₂ concentrations, including only the feedbacks acting on an ap-
 349 proximate 150-year timescale, i.e., assuming fixed ice sheets and vegetation. This met-
 350 ric, called “effective climate sensitivity” to distinguish it from true equilibrium, is termed
 351 S in SW20 [2] and hereafter. To infer S from Pliocene evidence, we build on SW20’s equa-
 352 tion of Pliocene energy balance by including the updates described below (distribution
 353 percentiles provided in Table S3).

$$\Delta T_{\text{Plio}} = \frac{-\Delta F_{\text{CO}_2} (1 + f_{\text{CH}_4}) + \Delta F_{\text{NonGHG}}}{\frac{\lambda_{2\text{xCO}_2}}{1+\zeta} + \Delta\lambda} \quad (5)$$

355 **(i)** Our main update is incorporating Pliocene $\Delta\lambda$ as $\Delta\lambda \sim \mathcal{N}(\mu = -0.37, \sigma =$
 356 $0.32) \text{ W m}^{-2} \text{ K}^{-1}$. We estimate μ and σ for $\Delta\lambda$ by combining the spread across AGCMs
 357 and reconstructions using the bootstrap approach in ref. [3], with plioDA’s best estimate
 358 as the reference value for differences in CAM4 and CAM5.

(ii) Pliocene forcing is updated based on the recent estimate of effective radiative forcing from non-GHG sources (ΔF_{NonGHG}), including ice sheets, vegetation, and land-sea distribution [23]. We assign $\Delta F_{\text{NonGHG}} \sim \mathcal{N}(1.7, 1.0) \text{ W m}^{-2} \text{ K}^{-1}$, which assumes a 1σ uncertainty that approximately maintains the original SW20 uncertainty in total ΔF_{Plio} . For reference, total ΔF_{Plio} (numerator of Eq. 5) is $3.9 \pm 1.2 (1\sigma) \text{ W m}^{-2}$, with $\Delta F_{\text{CO}_2} \approx 2.2 \text{ W m}^{-2}$. We note there is substantial uncertainty in the components of ΔF_{Plio} , which merit further study [17, 19, 53–57].

(iii) ΔT_{Plio} is updated from $3.0 \pm 1.0^\circ\text{C}$ (1σ) in SW20 to plioDA’s constraint of $\Delta T_{\text{Plio}} \sim \mathcal{N}(4.1, 0.6)^\circ\text{C}$ [5], which is supported by the estimate in ref. [6] of $3.9 \pm 1.1^\circ\text{C}$ (1σ).

From SW20 [2], the remaining parameters in Equation 5 are: CO₂ forcing of $\Delta F_{\text{CO}_2} = \Delta F_{2x\text{CO}_2} \times \ln(\frac{[\text{CO}_2]}{284\text{ppm}}) / \ln(2)$, where $[\text{CO}_2] \sim \mathcal{N}(375, 25) \text{ ppm}$ and $\Delta F_{2x\text{CO}_2} \sim \mathcal{N}(4.0, 0.3) \text{ W m}^{-2}$; a scaling factor for methane and N₂O forcing, $1+f_{CH_4}$, with $f_{CH_4} \sim \mathcal{N}(0.4, 0.1)$; and a timescale transfer factor between quasi-equilibrium and the 150-year S timescale, $1+\zeta$, to account for feedbacks becoming more positive at longer timescales, with $\zeta \sim \mathcal{N}(0.06, 0.2)$ based on LongRunMIP [31]. Finally, modern climate sensitivity is $S = -\Delta F_{2x\text{CO}_2} / \lambda_{2x\text{CO}_2}$ [2].

We also use an alternate version of the $\Delta\lambda$ in (i) estimated by comparing our paleoclimate AGCM simulations with feedbacks from 150-year regression of abrupt CO₂-forcing simulations in the parent coupled models of each AGCM. Each coupled model produces a distinct warming pattern, thereby sampling uncertainty in the pattern of warming from CO₂. With $\lambda_{150\text{yr}}^{\text{CO}_2}$ representing the regression feedback, we estimate Pliocene $\Delta\lambda_{150\text{yr}}^{\text{Alt}} = \lambda_{150\text{yr}}^{\text{CO}_2} - \lambda_{\text{Plio}}$, and we use the same bootstrap approach in (i) to find Pliocene $\Delta\lambda_{150\text{yr}}^{\text{Alt}} \sim \mathcal{N}(\mu = -0.44, \sigma = 0.40) \text{ W m}^{-2} \text{ K}^{-1}$. Because $\Delta\lambda_{150\text{yr}}^{\text{Alt}}$ represents a comparison with the 150-year regression feedback rather than quasi-equilibrium simulations, the denominator of Equation 5 becomes $(\lambda_{2x\text{CO}_2} + \Delta\lambda_{150\text{yr}}^{\text{Alt}}) / (1 + \zeta)$ when using $\Delta\lambda_{150\text{yr}}^{\text{Alt}}$ instead of our standard $\Delta\lambda$. Note that the percentiles of the final S distribution agree within 0.1°C when using $\Delta\lambda_{150\text{yr}}^{\text{Alt}}$ (Table S3).

There are advantages to our formulation of the Pliocene energy balance (Eq. 5) compared to SW20’s Equation 23. First, the Pliocene is now consistent with the LGM, as ΔF_{NonGHG} is now added directly rather than estimated by multiplying ΔF_{CO_2} by a scale factor, $1+f_{ESS}$, representing Earth system sensitivity [1, 27]. Second, f_{ESS} conflates forcings and feedbacks, and estimating f_{ESS} requires free-running coupled simulations that have inaccurate warming patterns [23]. Instead of using f_{ESS} , our Equation 5 separately includes *effective radiative forcing*, ΔF_{NonGHG} , from AGCM simulations with paleoenvironmental boundary conditions informed by proxies for ice extent, vegetation, and topography [23, 58], and *paleoclimate pattern effects*, from AGCM simulations with SST/SIC patterns constrained by data assimilation [3].

Climate sensitivity PDFs are summarized in Table S3. We calculate likelihoods and PDFs for S using SW20’s Bayesian framework [2]. This framework quantitatively combines our findings with additional lines of evidence, and the methods can be continually developed in ongoing efforts [59, 60]. Our findings would have the same directional impact on other assessments of ECS and modern warming [16, 61].

In Fig. 4 and Table S3, we show S with and without updates (i), (ii), and (iii). For the LGM evidence in Fig. 4b, we include updated $\Delta T_{\text{LGM}} \sim \mathcal{N}(-6, 1)^\circ\text{C}$ and LGM

403 $\Delta\lambda \sim \mathcal{N}(-0.37, 0.23) \text{ W m}^{-2} \text{ K}^{-1}$ [3]. We also use $\lambda_{150\text{yr}}^{\text{CO}_2}$ in Table S1 to estimate LGM
 404 $\Delta\lambda_{150\text{yr}}^{\text{Alt}} \sim \mathcal{N}(\mu = -0.42, \sigma = 0.34) \text{ W m}^{-2} \text{ K}^{-1}$. While SW20's framework generally
 405 assumes lines of evidence are independent, our estimates of Pliocene and LGM pattern
 406 effects are interrelated. We use the same AGCMs, and the reconstruction methods are
 407 partially overlapping. To account for the relationship between Pliocene and LGM $\Delta\lambda$
 408 estimates, we identify pairs of estimates that use similar reconstruction methods and the
 409 same AGCM (Table S4). From these pairs, we estimate the Pearson correlation (r) and
 410 covariance for $\Delta\lambda$ to be $r = 0.56$ and $\text{cov} = 0.0123 [\text{W m}^{-2} \text{ K}^{-1}]^2$. For $\Delta\lambda_{150\text{yr}}^{\text{Alt}}$, we
 411 estimate $r = 0.87$ and $\text{cov} = 0.0562 [\text{W m}^{-2} \text{ K}^{-1}]^2$. We account for the shared error
 412 covariance by drawing correlated values for LGM and Pliocene $\Delta\lambda$ from bivariate nor-
 413 mal distributions. However, the S constraints are insensitive to the covariance, as our
 414 Full Update percentiles (Table S3) change by less than 0.1°C if we assume zero covari-
 415 ance. This result aligns with the dependence tests in SW20, which also found relatively
 416 small impacts from codependencies [2].

417 We include results corresponding to SW20's robustness test, which assumes a uni-
 418 form prior on S from 0 to 20°C instead of the baseline prior of uniform λ from -10 to
 419 $10 \text{ W m}^{-2} \text{ K}^{-1}$, in Table S3. The robustness test yields a median of 3.1°C and 66% range
 420 of $2.6 - 3.8^\circ\text{C}$ (90% CI: $2.3 - 4.6^\circ\text{C}$). As for our main result using the baseline prior,
 421 this represents a substantial narrowing of uncertainty compared to the robust ranges in
 422 SW20. For illustrative purposes, we also include posterior PDFs considering only the Pliocene
 423 evidence and assuming the uniform- S prior. The PDF from the Pliocene alone has a me-
 424 dian of 3.8°C and 66% range of $2.4 - 7.2^\circ\text{C}$ (90% CI: $1.9 - 12.9^\circ\text{C}$).

425 Projections of 21st-century warming

426 We analyze warming projections through 2100 under SSP2-4.5 [16] from the FaIR
 427 model v1.4.1, calibrated to match historical records as in IPCC AR6 but with updated
 428 constraints through 2022 [47]. From FaIR, we have a large ensemble of global-mean tem-
 429 peratures from 1850–2100, and each member has an associated ECS. For each ensem-
 430 ble member, we compute the mean warming over 2081–2100 relative to the 1850–1900
 431 mean. We then resample the ensemble with replacement to match the specified ECS dis-
 432 tributions from SW20 and from our updated paleoclimate-constrained ECS. This resam-
 433 pling produces revised distributions of projected warming that are associated with the
 434 specified ECS distributions (Fig. 4).

435 Data availability

436 Model output and SST/SIC boundary conditions will be available on Zenodo upon
 437 publication. Pliocene reconstructions are available via refs. [5, 6]. Late Holocene recon-
 438 struction is available via ref. [8]. Effective radiative forcings for the Pliocene and mod-
 439 ern 2xCO_2 are available via ref. [23]. Results for LGM pattern effects are available via
 440 ref. [3]. LongRunMIP is available at longrunmip.org. CAM5 radiative kernels are avail-
 441 able via ref. [52]. Code for calculating ECS is available at doi.org/10.5281/zenodo.3945276 [2].

443 **Author contributions**

444 VTC performed the analysis, designed the experiments, wrote the original draft,
 445 and ran the simulations in CAM4, CAM5, and CAM6. KCA and GJH supervised the
 446 study. KCA, GJH, CP, JET, NJB, and VTC obtained funding and computing resources.
 447 JET and MBO contributed plioDA and LGMR reconstructions. TA ran HadGEM3 and
 448 WD ran GFDL-AM4 simulations. MTD and RF contributed Pliocene-forcing simula-
 449 tions. All authors contributed to editing the manuscript. All authors declare no com-
 450 peting interests.

451 **Acknowledgments**

452 Funding sources: National Defense Science & Engineering Graduate (NDSEG) Fellow-
 453 ship, U.S. Department of Defense (VTC); National Science Foundation (NSF) award OCE-
 454 2002276 (VTC, KCA, GJH, MTD); National Oceanic and Atmospheric Administration
 455 MAPP Program award NA20OAR431039 (KCA, CP, MTD); Alfred P. Sloan Research
 456 Fellowship grant FG-2020-13568 (KCA); NSF award OCE-2002398 (JET, MBO); NSF
 457 award OCE-2002385 (CP); NSF award OCE-2002448 (NJB); NSF award AGS-1844380
 458 (NJB); Met Office Hadley Centre Climate Programme funded by DSIT (TA); NSF award
 459 OCE-2103055 (RF); NSF award AGS-2238875 (RF). VTC acknowledges computing sup-
 460 port from Derecho (doi:10.5065/qx9a-pg09) and Casper (<https://ncar.pub/casper>)
 461 provided by the NSF National Center for Atmospheric Research (NCAR), sponsored by
 462 NSF. The authors thank Yi Ming and Dan Amrhein for helpful discussions and acknowl-
 463 edge NSF (No. 2238875) for funding a 2024 workshop on “Climate evolution from early
 464 Eocene to mid-Pliocene,” which helped shape this work.

465 **References**

- 466 [1] PALAEOSENS Project Members, Making sense of palaeoclimate sensitivity.
Nature **491**, 683–691 (2012).
- 467 [2] SC Sherwood, et al., An Assessment of Earth’s Climate Sensitivity Using Multi-
 468 ple Lines of Evidence. *Reviews of Geophysics* **58** (2020).
- 469 [3] VT Cooper, et al., Last Glacial Maximum pattern effects reduce climate sensi-
 470 tivity estimates. *Science Advances* **10**, 9461 (2024).
- 471 [4] KD Burke, et al., Pliocene and Eocene provide best analogs for near-future
 472 climates. *Proceedings of the National Academy of Sciences* **115**, 13288–13293
 473 (2018).
- 474 [5] JE Tierney, et al., Pliocene Warmth and Patterns of Climate Change Inferred
 475 From Paleoclimate Data Assimilation. *AGU Advances* **6** (2025).
- 476 [6] JD Annan, JC Hargreaves, T Mauritsen, E McClymont, SL Ho, Can we reli-
 477 ably reconstruct the mid-Pliocene Warm Period with sparse data and uncertain
 478 models? *Climate of the Past* **20**, 1989–1999 (2024).
- 479 [7] JE Tierney, et al., Glacial cooling and climate sensitivity revisited. *Nature* **584**,
 480 569–573 (2020).
- 481 [8] MB Osman, et al., Globally resolved surface temperatures since the Last
 482 Glacial Maximum. *Nature* **599**, 239–244 (2021).
- 483 [9] AM Seltzer, et al., Widespread six degrees Celsius cooling on land during the
 484 Last Glacial Maximum. *Nature* **593**, 228–232 (2021).

- [10] KC Armour, CM Bitz, GH Roe, Time-Varying Climate Sensitivity from Regional Feedbacks. *Journal of Climate* **26**, 4518–4534 (2013).
- [11] T Andrews, JM Gregory, MJ Webb, The Dependence of Radiative Forcing and Feedback on Evolving Patterns of Surface Temperature Change in Climate Models. *Journal of Climate* **28**, 1630–1648 (2015).
- [12] JM Gregory, T Andrews, Variation in climate sensitivity and feedback parameters during the historical period. *Geophysical Research Letters* **43**, 3911–3920 (2016).
- [13] P Ceppi, JM Gregory, Relationship of tropospheric stability to climate sensitivity and Earth’s observed radiation budget. *Proceedings of the National Academy of Sciences* **114**, 13126–13131 (2017).
- [14] T Andrews, MJ Webb, The Dependence of Global Cloud and Lapse Rate Feedbacks on the Spatial Structure of Tropical Pacific Warming. *Journal of Climate* **31**, 641–654 (2018).
- [15] E de la Vega, TB Chalk, PA Wilson, RP Bysani, GL Foster, Atmospheric CO₂ during the Mid-Piacenzian Warm Period and the M2 glaciation. *Scientific Reports* **10**, 11002 (2020).
- [16] P Forster, et al., 2021: The Earth’s energy budget, climate feedbacks, and climate sensitivity in *Climate Change 2021: The Physical Science Basis. Contribution of Working Group I to the Sixth Assessment Report of the Intergovernmental Panel on Climate Change*, eds. V Masson-Delmotte, et al. (Cambridge Univ. Press, Cambridge, UK and New York, NY), (2021).
- [17] PO Hopcroft, et al., Polar amplification of Pliocene climate by elevated trace gas radiative forcing. *Proceedings of the National Academy of Sciences* **117**, 23401–23407 (2020).
- [18] U Salzmann, et al., Challenges in quantifying Pliocene terrestrial warming revealed by data–model discord. *Nature Climate Change* **3**, 969–974 (2013).
- [19] H Dowsett, et al., The PRISM4 (mid-Piacenzian) paleoenvironmental reconstruction. *Climate of the Past* **12**, 1519–1538 (2016).
- [20] DJ Lunt, et al., On the causes of mid-Pliocene warmth and polar amplification. *Earth and Planetary Science Letters* **321–322**, 128–138 (2012).
- [21] JE Tierney, AM Haywood, R Feng, T Bhattacharya, BL Otto-Bliesner, Pliocene Warmth Consistent With Greenhouse Gas Forcing. *Geophysical Research Letters* **46**, 9136–9144 (2019).
- [22] LE Burton, et al., On the climatic influence of CO₂ forcing in the Pliocene. *Climate of the Past* **19**, 747–764 (2023).
- [23] M Dvorak, et al., Mid-Pliocene climate forcing, sea-surface temperature patterns, and implications for modern-day climate sensitivity. *Journal of Climate* (*in press*). (2025).
- [24] JE Weiffenbach, et al., Unraveling the mechanisms and implications of a stronger mid-Pliocene Atlantic Meridional Overturning Circulation (AMOC) in PlioMIP2. *Clim. Past* **19**, 61–85 (2023).
- [25] R Feng, et al., Past terrestrial hydroclimate sensitivity controlled by Earth system feedbacks. *Nature Communications* **13**, 1306 (2022).
- [26] S Menemenlis, JM Lora, M Lofverstrom, D Chandan, Influence of stationary waves on mid-Pliocene atmospheric rivers and hydroclimate. *Global and Plane-*

- 532 *tary Change* **204**, 103557 (2021).
- 533 [27] DJ Lunt, et al., Earth system sensitivity inferred from Pliocene modelling and
534 data. *Nature Geoscience* **3**, 60–64 (2010).
- 535 [28] GJ Hakim, et al., The last millennium climate reanalysis project: Framework
536 and first results. *Journal of Geophysical Research: Atmospheres* **121**, 6745–6764
537 (2016).
- 538 [29] R Caballero, M Huber, State-dependent climate sensitivity in past warm cli-
539 mates and its implications for future climate projections. *Proceedings of the*
540 *National Academy of Sciences* **110**, 14162–14167 (2013).
- 541 [30] I Eisenman, KC Armour, The radiative feedback continuum from Snowball
542 Earth to an ice-free hothouse. *Nature Communications* **15**, 6582 (2024).
- 543 [31] M Rugenstein, et al., LongRunMIP: Motivation and Design for a Large Col-
544 lection of Millennial-Length AOGCM Simulations. *Bulletin of the American*
545 *Meteorological Society* **100**, 2551–2570 (2019).
- 546 [32] DE Amrhein, GJ Hakim, LA Parsons, Quantifying Structural Uncertainty in
547 Paleoclimate Data Assimilation With an Application to the Last Millennium.
548 *Geophysical Research Letters* **47** (2020).
- 549 [33] AM Haywood, et al., The Pliocene Model Intercomparison Project Phase 2:
550 large-scale climate features and climate sensitivity. *Climate of the Past* **16**,
551 2095–2123 (2020).
- 552 [34] NJ Burls, AV Fedorov, What Controls the Mean East–West Sea Surface Tem-
553 perature Gradient in the Equatorial Pacific: The Role of Cloud Albedo. *Journal*
554 *of Climate* **27**, 2757–2778 (2014).
- 555 [35] E Erfani, NJ Burls, The Strength of Low-Cloud Feedbacks and Tropical Cli-
556 mate: A CESM Sensitivity Study. *Journal of Climate* **32**, 2497–2516 (2019).
- 557 [36] HL Ford, et al., Sustained mid-Pliocene warmth led to deep water formation in
558 the North Pacific. *Nature Geoscience* **15**, 658–663 (2022).
- 559 [37] EL McClymont, et al., Lessons from a high-CO₂ world: An ocean view from 3
560 million years ago. *Climate of the Past* **16**, 1599–1615 (2020).
- 561 [38] BJ Soden, et al., Quantifying Climate Feedbacks Using Radiative Kernels.
562 *Journal of Climate* **21**, 3504–3520 (2008).
- 563 [39] Y Dong, C Proistosescu, KC Armour, DS Battisti, Attributing Historical and
564 Future Evolution of Radiative Feedbacks to Regional Warming Patterns using a
565 Green’s Function Approach: The Preeminence of the Western Pacific. *Journal*
566 *of Climate* **32**, 5471–5491 (2019).
- 567 [40] MW Wara, AC Ravelo, ML Delaney, Permanent El Niño-Like Conditions Dur-
568 ing the Pliocene Warm Period. *Science* **309**, 758–761 (2005).
- 569 [41] AV Fedorov, et al., The Pliocene Paradox (Mechanisms for a Permanent El
570 Niño). *Science* **312**, 1485–1489 (2006).
- 571 [42] CL O’Brien, et al., High sea surface temperatures in tropical warm pools during
572 the Pliocene. *Nature Geoscience* **7**, 606–611 (2014).
- 573 [43] C Brierley, N Burls, C Ravelo, A Fedorov, Pliocene warmth and gradients. *Na-*
574 *ture Geoscience* **8**, 419–420 (2015).
- 575 [44] NJ Burls, AV Fedorov, Wetter subtropics in a warmer world: Contrasting past
576 and future hydrological cycles. *Proceedings of the National Academy of Sciences*
577 **114**, 12888–12893 (2017).

- 578 [45] JE Weiffenbach, et al., Highly stratified mid-Pliocene Southern Ocean in
579 PlioMIP2. *Climate of the Past* **20**, 1067–1086 (2024).
- 580 [46] C Wang, et al., Diagnosing the Factors That Contribute to the Intermodel
581 Spread of Climate Feedback in CMIP6. *Journal of Climate* **38**, 663–674 (2025).
- 582 [47] C Smith, et al., fair-calibrate v1.4.1: calibration, constraining, and validation of
583 the Fair simple climate model for reliable future climate projections. *Geoscientific
584 Model Development* **17**, 8569–8592 (2024).
- 585 [48] T Andrews, Using an AGCM to Diagnose Historical Effective Radiative Forcing
586 and Mechanisms of Recent Decadal Climate Change. *Journal of Climate* **27**,
587 1193–1209 (2014).
- 588 [49] G Danabasoglu, et al., The Community Earth System Model Version 2
589 (CESM2). *Journal of Advances in Modeling Earth Systems* **12** (2020).
- 590 [50] KD Williams, et al., The Met Office Global Coupled Model 3.0 and 3.1 (GC3.0
591 and GC3.1) Configurations. *Journal of Advances in Modeling Earth Systems*
592 **10**, 357–380 (2017).
- 593 [51] IM Held, et al., Structure and Performance of GFDL’s CM4.0 Climate Model.
594 *Journal of Advances in Modeling Earth Systems* **11**, 3691–3727 (2019).
- 595 [52] AG Pendergrass, A Conley, FM Vitt, Surface and top-of-atmosphere radiative
596 feedback kernels for CESM-CAM5. *Earth Syst. Sci. Data* **10**, 317–324 (2018).
- 597 [53] A Haywood, et al., Pliocene Model Intercomparison Project Phase 3
598 (PlioMIP3) – Science plan and experimental design. *Global and Planetary
599 Change* **232**, 104316 (2024).
- 600 [54] GR Grant, et al., The amplitude and origin of sea-level variability during the
601 Pliocene epoch. *Nature* **574**, 237–241 (2019).
- 602 [55] N Sagoo, T Storelvmo, Testing the sensitivity of past climates to the indirect
603 effects of dust. *Geophysical Research Letters* **44**, 5807–5817 (2017).
- 604 [56] A Dutton, et al., Sea-level rise due to polar ice-sheet mass loss during past
605 warm periods. *Science* **349** (2015).
- 606 [57] N Unger, X Yue, Strong chemistry-climate feedbacks in the Pliocene. *Geophysical
607 Research Letters* **41**, 527–533 (2014).
- 608 [58] J Zhu, CJ Poulsen, Last Glacial Maximum (LGM) climate forcing and ocean
609 dynamical feedback and their implications for estimating climate sensitivity.
610 *Climate of the Past* **17**, 253–267 (2021).
- 611 [59] K Marvel, M Webb, Towards robust community assessments of the Earth’s
612 climate sensitivity. *Earth System Dynamics* **16**, 317–332 (2025).
- 613 [60] SC Sherwood, CE Forest, Opinion: Can uncertainty in climate sensitivity be
614 narrowed further? *Atmospheric Chemistry and Physics* **24**, 2679–2686 (2024).
- 615 [61] D Kaufman, V Masson-Delmotte, Opinion: Distribute paleoscience information
616 across the next Intergovernmental Panel on Climate Change reports. *Climate of
617 the Past* **20**, 2587–2594 (2024).